Calculated Structures of MO_2^{2+}, MN_2, and MP_2 (M = Mo, W)

Pekka Pyykkö*,† and Toomas Tamm*,‡

Department of Chemistry, PL 55 (A. I. Virtasen aukio 1), FIN-00014, University of Helsinki, Finland

Received: May 7, 1997; In Final Form: August 6, 1997[⊗]

Ab initio calculations of MoN_2, MoP_2, MoO_2^{2+} WN_2, WP_2, and WO_2^{2+} were performed using quasi-relativistic effective core potentials and MP2, B3LYP, CCSD(T) and CASPT2 methodologies. Multiple local minima were found on the potential energy surfaces of the various spin states of the nitrides and phosphides. The nitrides all are either above the dissociation limit or only very slightly below it. The phosphides are energetically below the dissociation limit. The bond angles of the oxoions, as well as the phosphides and nitrides at some spin states, are nearly tetrahedral. Several minima with narrow (35−65°) bond angles, representing a side-on bond of a partially dissociated N_2 or P_2 molecule to the metal atom, were found as well. The oxoions and phosphides are believed to have an autonomous, gas-phase existence. The character of the bonding molecular orbitals has been analyzed.

1. Introduction

The oxide halides and oxo organometallic complexes of hexavalent molybdenum or tungsten (M = Mo, W) commonly occur[1−3] as MO_2X_2 groups, where X is a halogen or organic ligand. It is customary in inorganic chemistry to see them as halides of an MO_2^{2+} group, called molybdenyl or tungstenyl. Does this group actually exist in free form?

Tatsumi and Hoffmann[4] have analyzed, at the extended Hückel (EHT) level, the reasons for its roughly tetrahedral O−M−O bond angle of 102−114°. We are not aware of any ab initio calculations or experimental studies on the free M(VI)-O_2^{2+} groups, M = Mo,W. Earlier calculations do exist for the entire MoO_2X_2 series.[5] The related gas-phase CrO_2^+ species has been observed.[6] It is interesting that the CrO_2^{2+} groups in gas-phase CrO_2F_2 and in the solid CrO_2F_2 with a fluorine layer structure have closely similar O−Cr−O angles[7] of 102 degrees.

Further, we wanted to study the isoelectronic neutral molecules MN_2 and MP_2, originally in the hope that they would provide useful, simple models for the M≡N and M≡P bonds in the nitrides or phosphides of group 6 metals. Recently, molecular examples of such compounds have been reported.[8,9] Again, EHT calculations[10] and ab initio work[11,12] have been reported for larger molecules but not on the simplified MN_2 or MP_2 systems.

While this work was in progress, the results of Martínez, Köster, and Salahub[13] were published, providing a thorough nonrelativistic density functional theory (DFT) study of MoN_2. These results are directly comparable with ours, and such comparisons will be made where applicable.

Experimentally, all of the nitrides and phosphides studied are known in the solid phase (the physical constants can be found, e.g., ref 14, pp 4-77 and 4-109). Very little experimental data is available about these species in gas phase or matrixes. Foosnaes et al.[15] have studied molybdenum−dinitrogen complexes in krypton matrixes. A weakly bound complex was observed, but no detailed geometrical structure could be deduced from the experimental data. Flow-tube kinetic studies[16] revealed no reactivity between Mo or Mo_2 and N_2 in the gas phase.

To our surprise, the computational results give evidence that there exist several local minima on the potential energy surfaces (PES) of the MN_2 and MP_2. Some have large X−M−X angles, while the angles in the rest are small. Typical values are 96−97° and 45−65°, respectively. The latter exhibit remaining N−N or P−P bonding. Goldberg et al.[17] quote only one experimentally known example of such a side-on, η^2- N_2 complex, to a single metal atom, in (η -C_5H_4R')$_2$Zr(N_2)R. For instance, NFeN has an experimentally estimated bond angle of 115(±5)°.[18] Calculations give 114°[18] or 40.[19] A brief discussion on side-on N_2 complexing can also be found on p 162 of ref 20.

Before completion of our work, we became aware of a so-far unpublished matrix spectroscopic observation of a large-angle MoN_2 species of unknown spin.[21]

2. Method

Basis Sets and Pseudopotentials. Most of the calculations were performed using the Molcas 3[22] and Gaussian 94[23] programs. For the Molcas calculations, the Stuttgart quasi-relativistic pseudopotentials (effective core potentials) and basis sets[24] were used for Mo, W, and P. The nonrelativistic Dunning/Huzinaga[25] double-ζ basis sets were used for N and O. The latter choice was made so that the same basis set could be used in both the Molcas and Gaussian calculations. In the Gaussian 94, the small-core Los Alamos ("LANL2DZ") pseudopotentials and basis sets[26] were employed. Since the corresponding parametrizations are not available for the second-row elements (N, O), the Dunning/Huzinaga[25] double-ζ basis is automatically selected by the Gaussian 94 program for these elements, and we preferred to use the same basis in the Molcas calculations as well.

All basis sets were augmented with a set of seven f (for Mo, W) or five d (N, O, P) polarization functions, with the exponents chosen from the works of Ehlers et al.[27] and Huzinaga et al.[28] The exponents are given in Table 1. For the case of MoN_2, the basis set completeness was probed at the MP2 level by adding two more sets of f functions to the metal [one diffuse (α = 0.3477) and one tight (α = 3.129)], with no appreciable changes in the results.

Electron Correlation. Initially, the correlation effects were treated at the level of second-order Møller−Plesset perturbation theory (MP2) or using coupled clusters with single and double

* Authors to whom correspondence should be addressed.
† e-mail: Pekka.Pyykko@helsinki.fi.
‡ e-mail: toomas@chem.helsinki.fi.
⊗ Abstract published in *Advance ACS Abstracts,* October 1, 1997.

S1089-5639(97)01537-5 CCC: $14.00

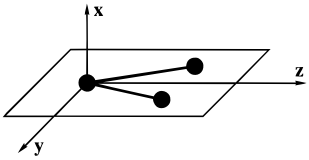

Figure 1. Coordinate system used in this work. A p_x orbital would transform as B_2.

TABLE 1: Exponents of Polarization Functions Used in This Work

element	type of function	exponent	ref
N	d	0.864	28
O	d	1.154	28
P	d	0.340	28
Mo	f	1.043	27
W	f	0.823	27

excitations, including triples perturbatively [CCSD(T)]. Alternatively, we performed density functional theory (DFT) calculations with the B3LYP exchange-correlation functional. All these calculations are based on a single closed-shell RHF reference state. It was found, however, that the nitrides and phosphides cannot be reliably described at the single-reference level (the Results section contains a more detailed analysis).

Therefore, multireference CASPT2[29,30] calculations were performed using Molcas 3. Parallel calculations were performed with all reasonable values of the total spin, (S): 0, 1, 2, and 3. The active space was chosen to include at least two orbitals (highest occupied and lowest unoccupied of an $S = 0$ RHF treatment) in each irreducible representation (eight orbitals total). This active space appeared, however, to be inadequate, especially in describing the high-spin states. The best-quality results were obtained by using an active space of five or six a_1, two or three b_1, three b_2, and two a_2 orbitals (C_{2v} symmetry; the coordinate system is illustrated in Figure 1). Inclusion of more than 13 orbitals would have been desirable in some cases, but the computational cost of the calculations would have become prohibitive.

Geometry Optimizations. In the Gaussian 94 calculations, they were done with the Fletcher−Powell algorithm with numerical derivatives. The Gaussian 94 default, Berne algorithm, does not handle pseudopotentials; neither are analytical derivatives available for all systems studied. The sharp potential energy curve of the N_2 molecule, and its intramolecular counterpart in some of the systems investigated, called for modification of the default step sizes for numerical differentiation. Typically $^1/_2$ to $^1/_4$ of the program defaults had to be used in order to achieve convergence in geometries.

In the Molcas calculations, where derivatives of the CASPT2 energy are not available, the geometries were optimized using a simple nongradient algorithm developed for this project. The algorithm makes trial calculations around a starting point along the coordinate axes and then changes the geometry along the coordinate that leads to biggest decrease in energy. The step size (both for probing and stepping) is adjustable, but it will not drop below a predetermined minimum until trials in all directions lead to energy increase. At this point, the step size is divided by 10, and the procedure repeated. Convergence is achieved when the step size falls below a given threshold, 0.001 bohr in the current calculations.

For each state, several starting geometries (wide-angle and small-angle, as well as linear) were considered. In most cases, the different initial bond angles lead to the same minimum, but sometimes there are several local minima. In such cases, the lowest energy minimum for each symmetry is reported.

Whenever a CASPT2 minimum had been located, single-point calculations were performed for alternative electronic states with the same spin and other spatial symmetries of the wave function. If any of those yielded a lower energy, optimization was continued from the geometry obtained, using the new electronic state.

Most of the geometry optimizations were carried out within the constraints of C_{2v} or $C_{\infty v}$ symmetry. The numerical Hessians were calculated at the stationary points for the Gaussian 94 calculations to prove that true minima had been reached. Calculations of all the second derivatives for the various minima on the CASPT2 PES would have been computationally very expensive. There are also no algorithms supplied with Molcas-3 for automation of this task. Therefore, several PES scans were performed, and alternate geometries and symmetries were checked near the minimum geometries. The presented stationary points are believed to be local minima on the corresponding potential energy surfaces.

For several combinations of chemical composition and total spin, the active space used in the CASPT2 calculations was inadequate for a proper description of the bonding. The so-called intruder states, states not contained in the CAS configuration function space, which at certain geometries become degenerate with the CASSF wave function,[31] lead to singularities on the PES. In many cases, these can be circumvented by suitably modifying the active space. However, in some cases the only option would be to add further orbitals into the active space, thus making the calculation prohibitively expensive. We also attempted to use the same active space for all spin values of a given compound, to improve the comparability of the energies. If no other way to avoid the singularities could be found, the energies and geometries were extrapolated manually from calculated points around the singularity and then the automatic minimization was allowed to continue.

Visualization. The final CASPT2 natural orbitals of MoN_2 were normalized and plotted on a grid, and the isosurfaces on the grid data were visualized using AVS.[32] The figures in this paper represent the surfaces where the absolute value of the wave function equals 0.09 $(a_0)^{-3/2}$, where a_0 is the Bohr radius.

3. Results

The optimized geometries are given separately in Tables 2 and 3 for the single-reference and multireference methods, respectively. Vibrational frequencies are given at single-reference level only, in Table 4. The calculated distances and frequencies are compared with experimental ones for related systems with M≡X bonds in Table 5. The CASPT2 structures are illustrated in Figures 2−5. The calculated vibrational frequencies could be useful in identifying these species in gas-phase or matrix experiments, even though they correspond to the closed-shell treatment of the systems.

Correlation effects appear to be very important in treating these systems. Initially, attempts were made to use single-reference methods [MP2, B3LYP, CCSD(T)]. The lack of consistency for some of the geometries, however, prompted a further investigation on the nature of the bonding in these molecules. It appears that both static and dynamic correlation effects need to be taken into account for a proper description of the systems.

Also, the single-reference Gaussian 94 calculations always converged to the totally symmetric $^1A_1$ electronic state, while later CASPT2 calculations revealed that several of these systems possess the B_2 symmetry in the singlet state. This may explain some of the differences between the single-reference and multireference results.

TABLE 2: Optimized Geometries from Single-Reference Calculations (in picometers and degrees)[a]

system	2S +1	method	M−X (pm)	X−X (pm)	X−M−X (deg)
MoN_2	1	HF	210.2	113.6	31.4
	1	MP2	175.5	164.0	55.7
	1	MP2[b]	174.0	164.5	56.4
	1	B3LYP	166.0	264.0	104.5
	1	CCSD(T)	168.4	266.1	104.4
WN_2	1	MP2	176.0	168.4	57.2
	1	B3LYP	174.9	149.3	50.5
	1	CCSD(T)[c]	174.9	156.5	53.2
	1	CCSD(T)	170.7	270.3	104.7
MoP_2	1	MP2	209.9	330.2	103.7
	1	B3LYP	214.2	340.8	105.4
	1	CCSD(T)	221.0	228.4	62.2
WP_2	1	HF	212.9	338.9	105.5
	1	MP2	217.4	343.7	104.4
	1	B3LYP	218.4	231.1	63.9
	1	CCSD(T)	219.6	236.2	65.1
MoO_2^{2+}	1	MP2	163.1	251.0	100.6
	1	B3LYP	161.8	249.7	101.0
	1	CCSD(T)	163.5	252.1	100.9
WO_2^{2+}	1	MP2	165.7	256.2	101.3
	1	B3LYP	163.6	253.4	101.5
	1	CCSD(T)	164.9	255.1	101.4

[a] LANL2DZ pseudopotential and basis sets except where noted. $^1A_1$ state in all cases. [b] Stuttgart basis and ECP. [c] Two minima were found, the narrow-angle one lying 2.3 kcal/mol lower.

One of the indicators of the quality of description of the systems at the CCSD level of theory is the Lee and Taylor T_1 diagnostic[33]

$$T_1 = \frac{||t_1||}{N_{\text{elec}}^{1/2}} \quad (1)$$

where $||t_1||$ is the Euclidean norm of the vector of t_1 amplitudes, and N_{elec} is the number of correlated electrons. The t_1 amplitudes in coupled-cluster theory are closely related to the coefficients of singly excited configurations in configuration interaction theory.

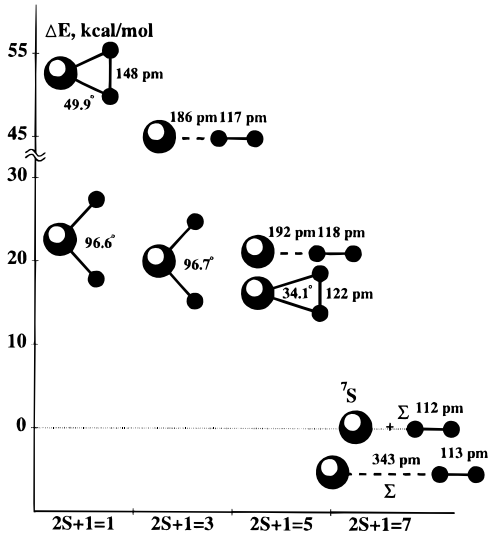

Figure 2. CASPT2 optimized geometries of MoN_2. All bent species have B_2, and the unmarked linear species have Π spatial symmetry of the electronic wave function.

A description is considered to be good at the CCSD level if $T_1 < 0.02$. Slightly larger values are permissible when the triples correction is taken into account. For our systems, $T_1 = 0.035-0.038$ for the oxoions and WN_2, $T_1 \approx 0.1$ for the phosphides, and $T_1 \geq 0.3$ for MoN_2 at the narrow-angle geometries. This indicates that that the descriptions of MoN_2, MoP_2 and WP_2 are not necessarily reliable at the CCSD(T) level and very likely not at the level of any computationally feasible single-reference method.

Therefore, all the systems were investigated further with the CASPT2 method, using the Molcas 3 program package and

TABLE 3: Optimized Geometries from CASPT2 Calculations (in pm and deg) and Energies Relative to Isolated Metal Atom and N_2 or P_2 (kcal/mol)[a]

system	2S + 1	state	M−X (pm)	X−X (pm)	X−M−X (deg)	energy	dominant configuration[b]
MoN_2	1	$^1A_1$	175.7	148.2	49.9	+53.1	$(5a_1)^2(6a_1)^2(1a_2)^2(2b_1)^2(4b_2)^2(5b_2)^2$
	1	$^1B_2$	171.7	256.2	96.6	+22.6	$(5a_1)^2(6a_1)^2(7a_1)^1(1a_2)^2(2b_1)^2(4b_2)^2(5b_2)^1$
	3	$^3B_2$	170.1	254.9	96.7	+20.0	$(5a_1)^2(6a_1)^2(7a_1)^1(1a_2)^2(2b_1)^2(4b_2)^2(5b_2)^1$
	3	$^3\Pi$	186.3	117.2	linear[c]	+44.9	$(7\sigma)^2(8\sigma)^1(9\sigma)^1(3\pi)^2(4\pi)^2(5\pi)^2(6\pi)^1(1\delta)^1$
	5	$^5B_2$	208.2	122.1	34.1	+16.3	$(5a_1)^2(6a_1)^2(7a_1)^1(8a_1)^1(1a_2)^1(2b_1)^2(3b_1)^1(4b_2)^2$
	5	$^5\Pi$	191.6	117.9	linear	+21.2	$(7\sigma)^2(8\sigma)^1(9\sigma)^1(3\pi)^2(4\pi)^2(5\pi)^2(6\pi)^1(1\delta)^1$
	7	$^7\Sigma$	343.3	113.2	linear	−4.9	$(7\sigma)^2(8\sigma)^1(9\sigma)^1(10\sigma)^1(3\pi)^2(4\pi)^2(5\pi)^1(6\pi)^1(1\delta)^1$
WN_2	1	$^1A_1$	176.2	157.7	53.2	+25.1	$(5a_1)^2(6a_1)^2(7a_1)^2(1a_2)^2(2b_1)^2(4b_2)^2$
	1	$^1B_2$	174.6	260.2	96.4	−5.7	$(5a_1)^2(6a_1)^2(7a_1)^1(1a_2)^2(2b_1)^2(4b_2)^2(5b_2)^1$
	1	$^1\Pi$	184.8	118.0	linear	+41.1	$(7\sigma)^2(8\sigma)^2(3\pi)^2(4\pi)^2(5\pi)^2(6\pi)^2$
	3	$^3B_2$	173.8	261.1	97.4	−3.5	$(5a_1)^2(6a_1)^2(7a_1)^1(8a_1)^1(1a_2)^1(2b_1)^2(3b_1)^1(4b_2)^2$
	5	$^5\Sigma$	196.5	115.3	linear	+10.0	$(7\sigma)^2(8\sigma)^2(9\sigma)^1(3\pi)^2(4\pi)^2(5\pi)^1(6\pi)^1(1\delta)^1$
MoP_2	1	$^1A_1$	218.0	351.3	107.4	−1.6	$(5a_1)^2(6a_1)^2(1a_2)^2(2b_1)^2(4b_2)^2(5b_2)^2$
	1	$^1B_2$	220.4	330.6	97.2	−30.0	$(5a_1)^2(6a_1)^2(7a_1)^1(1a_2)^2(2b_1)^2(4b_2)^2(5b_2)^1$
	3	$^3A_1$	229.4	228.0	60.1	−27.1	$(5a_1)^2(6a_1)^2(7a_1)^1(8a_1)^1(1a_2)^2(2b_1)^2(4b_2)^2$
	3	$^3B_2$	219.0	326.7	96.5	−25.7	$(5a_1)^2(6a_1)^2(7a_1)^1(1a_2)^2(2b_1)^2(4b_2)^2(5b_2)^1$
	5	$^5B_2$	242.8	209.6	51.1	−35.1	$(5a_1)^2(6a_1)^2(7a_1)^1(8a_1)^1(1a_2)^1(2b_1)^2(3b_1)^1(4b_2)^2$
	7	$^7B_2$	262.7	208.7	46.8	−5.1	$(5a_1)^2(6a_1)^2(7a_1)^1(8a_1)^1(1a_2)^1(2b_1)^2(3b_1)^1(4b_2)^1(5b_2)^1$
WP_2	1	$^1A_1$	220.5	235.8	64.7	−36.7	$(5a_1)^2(6a_1)^2(7a_1)^2(1a_2)^2(2b_1)^2(4b_2)^2$
	1	$^1B_2$	217.1	283.0	92.8	−49.6	$(5a_1)^2(6a_1)^2(7a_1)^1(1a_2)^2(2b_1)^2(4b_2)^2(5b_2)^1$
	3	$^3B_1$	222.6	235.6	63.9	−35.7	$(5a_1)^2(6a_1)^2(7a_1)^1(1a_2)^2(2b_1)^2(3b_1)^1(4b_2)^2$
	3	$^3B_2$	219.3	322.7	94.7	−46.8	$(5a_1)^2(6a_1)^2(7a_1)^1(1a_2)^2(2b_1)^2(4b_2)^2(5b_2)^1$
	5	$^5B_2$	228.6	382.9	113.8	−19.4	$(5a_1)^2(6a_1)^2(7a_1)^1(1a_2)^2(2b_1)^1(3b_1)^1(4b_2)^2(5b_2)^1$
MoO_2^{2+}	1	$^1A_1$	164.6	255.3	101.7		$(5a_1)^2(6a_1)^2(1a_2)^2(2b_1)^2(4b_2)^2(5b_2)^2$
WO_2^{2+}	1	$^1A_1$	166.9	258.1	101.4		$(5a_1)^2(6a_1)^2(1a_2)^2(2b_1)^2(4b_2)^2(5b_2)^2$

[a] Stuttgart pseudopotentials and basis sets. [b] The use of pseudopotentials for phosphorus atoms and all-electron basis sets for nitrogen and oxygen atoms actually introduces different labels for analogous valence orbitals. For consistent identification, we started the orbital count at $2a_1$ and $2b_1$ for MP_2 species. [c] Geometries marked as "linear" correspond to end-on alignment of N_2 toward Mo or W.

TABLE 4: Vibrational Frequencies (in cm^{-1}) for $^1A_1$ States[a]

system	method	$\nu_1(a_1)$	$\nu_2(a_1)$	$\nu_3(b_2)$
MoN_2	HF	2126	304	464
	MP2	1014	843	939
	MP2[b]	994	845	990
	B3LYP	1090	482	930
	CCSD(T)	**1025**	**461**	**896**
WN_2	MP2	1083	949	964
	B3LYP	1094	231	912
	CCSD(T)[c]	**1040**	**246**	**898**
	CCSD(T)[d]	**1025**	**431**	**970**
MoP_2	MP2	708	269	884
	B3LYP	544	213	533
	CCSD(T)	**516**	**310**	**440**
WP_2	HF	591	199	536
	MP2	590	203	640
	B3LYP	555	193	474
	CCSD(T)	**510**	**233**	**466**
MoO_2^{2+}	MP2	1673	497	2046
	B3LYP	1121	468	1062
	CCSD(T)	**1027**	**453**	**946**
WO_2^{2+}	MP2	1230	443	1468
	B3LYP	1133	445	1078
	CCSD(T)	**1074**	**433**	**1022**

[a] LANL2DZ pseudopotential and basis were used unless otherwise noted. The isotopes ^{14}N and ^{98}Mo were assumed. The values that we trust most for each particular species are printed in bold. [b] Stuttgart basis and ECP. [c] N−W−N angle = 53.2°. [d] N−W−N angle = 104.7°.

TABLE 5: Comparison of the Present CASPT2 Bond Lengths (R) and CCSD(T) Stretching Vibrational Frequencies (ν) with Those in ≡M≡E Mononitrides and Phosphides (R in pm, ν in cm^{-1})

bond	species	property	this work[a]	exptl	ref
W≡^{14}N	$^1A_1$ WN_2	ν	1025	1015[b]	34
Mo≡P	$^1B_2$ MoP_2	R	220.4	211.9[c]	8
Mo≡P	$^1A_1$ MoP_2	ν	516	521[d]	34
W≡P	$^1B_2$ WP_2	R	217.1	216.2[e]	9
W≡P	$^1A_1$ WP_2	ν	510	516[e]	34

[a] Tables 3 and 4. [b] In $[(Me_3SiNCH_2CH_2)_3N]W{\equiv}N$. [c] In Mo(P)(N-RAr)$_3$. [d] In $[(Me_3SiNCH_2CH_2)_3N]Mo{\equiv}P$. [e] In $[(Me_3SiNCH_2CH_2)_3N]$-W≡P.

considering all realistic total spin values (0, 1, 2, and 3). The obtained results are presented in the following subsections.

MoN_2. Our CASPT2 results for this species are similar to those obtained by Martínez et al.[13] using nonrelativistic DFT methodology. There are, however, some differences, which will be pointed out below. We also acknowledge the adoption of their style of graphical presentation in our Figures 2−5.

Except for the weakly bound septet ($2S+1 = 7$) linear complex, all the minima on the PES of MoN_2 lie above the dissociation limit. The B_2 quintet ($2S+1 = 5$) complex is a narrow-angled triangle, which essentially represents a side-on chemical bond to a partially dissociated N_2 molecule. The DFT calculations of Martínez et al. suggest that this structure might even be lower in energy than the isolated Mo and N_2, while we find it to be 16 kcal/mol above the dissociation limit. Their comments about the current DFT functionals overbinding weakly bound systems may thus be justified. They also list a bound linear quintet complex, which we failed to find. Instead, we find a septet linear system with similar energy, and with a very long N−Mo distance (343 pm), as well as a quintet linear system with an energy higher than that of the triangular quintet. We suggest that either of these quintet or septet complexes could have been observed in the experiments of Foosnaes et al.[15]

The singlet and triplet B_2 complexes are relatively high in energy with relation to the dissociation limit. (21−22 kcal/mol in this work, 6−11 kcal/mol in ref 13). We found the singlet to possess B_2 symmetry, while Martinez et al. list it as A_1. (In our calculations, the molecule was in the *YZ* plane, with *z*-axis being the axis of rotation (Figure 1), and the off-plane p_x orbital transforming as B_2. The study of Martínez et al. is using an alternative coordinate system, and their B_1 symmetry corresponds to our B_2.) The experiments by Andrews et al.[21] probably saw MoN_2 in the singlet or triplet B_2 state. The vibrational frequencies of singlet $^1A_1$ MoN_2 were calculated at the CCSD(T) level and are available in Table 4.

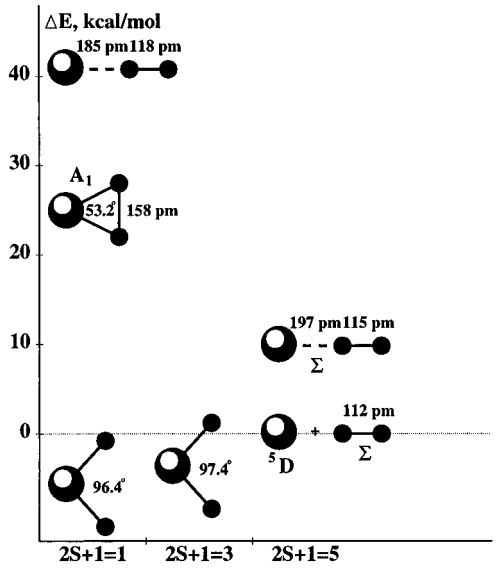

Figure 3. CASPT2 optimized geometries of WN_2. Unmarked bent species have B_2, and unmarked linear species have Π spatial symmetry of the electronic wave function.

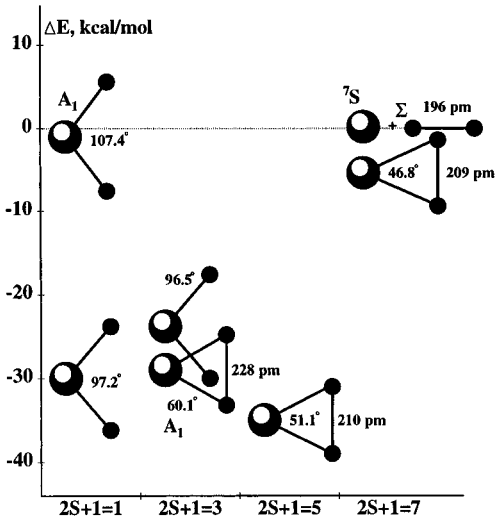

Figure 4. CASPT2 optimized geometries of MoP_2. All unmarked species have B_2 spatial symmetry of the electronic wave function. The energy difference between the two triplet states is exaggerated.

WN_2. Since Molcas 3 is not able to take into account spin−orbit splitting, and the 5D ground state of the tungsten atom is split into five levels as far as 6219 cm^{-1} apart, it was not possible to directly calculate the energy of the $^5D_0$ ground state of W atom with the means at our disposal without referring to experimental data. On the other hand, the ^7S first excited state can be calculated easily at the CASPT2 level. Therefore we estimated the energy of the $^5D_0$ ground state of W from the calculated energy of ^7S W and the experimental transition energy (2951.29 cm^{-1})[37] between these two states. As a result, the comparison of the energies with the dissociation limit is partially empirical.

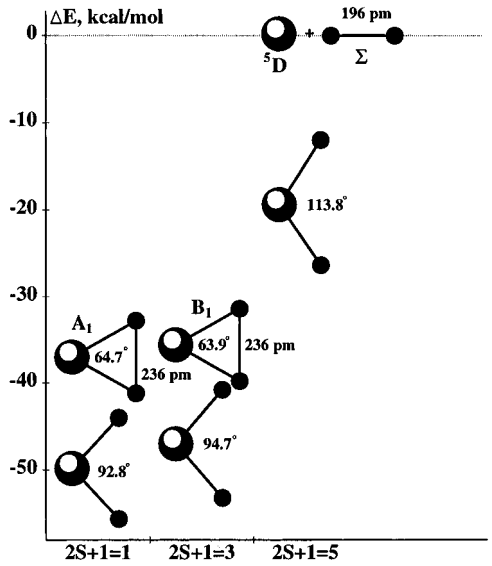

Figure 5. CASPT2 optimized geometries of WP_2. All unmarked species have B_2 spatial symmetry of the electronic wave function.

There appear to be no stable septet structures of WN_2. We did find a linear quintet complex at +10 kcal/mol from our estimated dissociation limit. Similar to MoN_2, we found singlet and triplet B_2 wide-angle minima. In this case, they are 3−6 kcal/mol below the dissociation limit and about 15 kcal/mol below the weakly bound quintet complex. A narrow-angle and a linear singlet geometry were found as well, but these are situated 25−40 kcal/mol above the quintet systems and therefore have little interest.

We suggest that the singlet and/or triplet systems could be experimentally produced in rare-gas matrixes, and possibly even in the gas phase. CCSD(T) vibrational frequencies of $^1A_1$ WN_2 are presented in Table 4. Comparison of the W−N stretching frequency in the wide-angle singlet with the experimental one in [$(Me_3$ $SiNCH_2$ $CH_2)_3$ N]W≡N (Table 5) appears to indicate that the bonding in WN_2 is similar to that in the large complex.

MoP_2. Just like the nitrides, the phosphides have wide-angle (over 90°) structures at lower spins (singlets and triplets). MoP_2 has a clear tendency toward narrow-angle structures at higher spins, with near or less than 60° bond angles found in triplet, quintet, and septet states. The almost equilateral triangular $^3A_1$ triplet configuration is very close in energy to the wide-angle $^3B_2$ state. The energetic difference between these two is only 1.4 kcal/mol.

In contrast to the nitrides, all minima are located below the dissociation limit. The calculated bond lengths and stretching frequencies are similar to the experimental ones in Mo(P)-$(NRAr)_3$ and [$(Me_3SiNCH_2$ $CH_2)_3$ N]Mo≡P, respectively (Table 5). We predict that molecular MoP_2 should be observable both in gas-phase and in rare-gas matrixes.

WP_2. The calculated minimum geometry of this species is very highly dependent on the computational procedure, spin-state, and symmetry involved. CCSD(T) and B3LYP predict a small (64−65°) and MP2 a large (104°) singlet bond angle. With any of the methods, the energetic difference between the "wide" and "narrow" geometries is relatively small. At the CASPT2 level, both the narrow- and wide-angle species are present on both the singlet and triplet surfaces. This molecule is also the only one that has a B_1 state among the stable ones (the narrow-angle triplet). As an additional surprise, we found a relatively high-lying, but still bound, quintet structure with the largest bond angle in any of the systems studied: 113.8°.

Again, the exact energy of the dissociation limit could not be calculated, but with the systems lying 30−50 kcal/mol below the estimated dissociation limit, we have little doubt that WP_2 could be observed experimentally in the gas phase as well as in matrixes. The bond lengths and stretching frequencies are, again, very similar to experimental ones of W≡P triple bonds.

TABLE 6: Comparison of the Present CASPT2 M−O Bond Lengths (R), O−M−O Angles (θ), and CCSD(T) Vibrational Frequencies (ν) with Those in Gaseous and Solid Oxide Halides of Molybdenum and Tungsten

species	property	this work[a]	exptl compound	exptl value	ref
$^1A_1$ MoO_2^{2+}	R	164.6 pm	MoO_2Cl_2 (gas)	168.6	35
$^1A_1$ MoO_2^{2+}	θ	101.7°	MoO_2Cl_2 (gas)	106.3°	35
$^1A_1$ MoO_2^{2+}	ν_1 (a_1)	1027 cm^{-1}	MoO_2Cl_2 (gas)	996 cm^{-1}	35
$^1A_1$ MoO_2^{2+}	ν_2 (a_1)	453 cm^{-1}	MoO_2Cl_2 (gas)	338 cm^{-1}	35
$^1A_1$ MoO_2^{2+}	ν_3 (b_2)	946 cm^{-1}	MoO_2Cl_2 (gas)	970 cm^{-1}	35
$^1A_1$ WO_2^{2+}	R	166.9 pm	WO_2Cl_2 (solid)	166.4 pm[b]	36
$^1A_1$ WO_2^{2+}	θ	101.4°	WO_2Cl_2 (solid)	101.9°	36

[a] Table 3. [b] Average of 170.2 and 162.9 pm, the two short bonds in the polymeric WO_2^{2+} structure.

MoO_2^{2+} and WO_2^{2+}. In contrast to their isoelectronic neutral counterparts, these ions behave very well already in the single-reference calculations. All methods we used predict them to have bond angles of about 101°. Both species are $^1A_1$ singlets, with other spin states and symmetries lying over 50 kcal/mol higher. The calculated bond lengths, bond angles, and frequencies compare favorably with experimental values in gas-phase MoO_2Cl_2, as well as solid WO_2Cl_2 (Table 6). One should still keep in mind, though, that the energetic cost (ΔH) of making a doubly ionized MoO_2^{2+} out of ^7S Mo and $^3\Sigma$ O_2 is 18.3 eV, which means that the system represents a local minimum on the top of a high "hill" on the potential energy surface. The analogous value for WO_2^{2+} is 9.8 eV. On the other hand, since the ions themselves are closed-shell singlets, several spin flips would be required to reach the dissociation limit. This makes it reasonable to expect a rather large barrier to dissociation. We believe that experimental observation of "free" molybdenyl and tungstenyl groups in the gas phase could be possible.

4. Bonding Analysis

The ground states of the Mo and W atoms are $4d^55s^1$ and $5d^46s^2$, respectively. The bonding in the present dinitrides can be understood by considering the interaction of these metal atoms with the nitrogen 2p shell, leading to a 12-electron problem. In the narrow-angle case, such as the lower MoN_2 quintet in Figure 2, the nitrogen part is close to an N_2 molecule. In the wide-angle case, like the lower MoN_2 singlets and triplets in Figure 2, local M−N multiple bonds offer a better description. The molecules containing W or having P and O ligands fall into these general cases.

The Narrow-Angle Case. The isodensity surfaces for the lower quintet state of MoN_2 are shown in Figure 6 and the orbitals are classified in Table 7. The 12 valence electrons essentially occupy the $(5a_1)^2(6a_1)^2(2b_1)^2(4b_2)^2(7a_1)^1(8a_1)^1(1a_2)^1$-$(3b_1)^1$ (the exact CASPT2 occupation numbers are 1.97, 1.81, 1.78, 1.69, 0.95, 0.93, 0.94, 0.94). As the C_{2v} a_2b_1=b_2, a $^5B_2$ state is obtained. As seen from the figure, the $5a_1$ forms the N−N 2pσ bond, the $6a_1$ the N−N in-plane 2pπ bond, and the $2b_1$ the N−N off-plane 2pπ bond. The $4b_2$ MO involves the Mo $4d_{yz}$ and the N_2 in-plane 2pπ* MO. It makes Mo−N σ bonds and partially breaks the in-plane 2pπ N−N bond (Figure 7).

Of the four singly occupied MOs, the $3b_1$ is a Mo $4d_{xz}$, slightly bonding with the N_2 off-plane π. The remaining three Mo 4d AO's (y^2, $z^2 - x^2$, and xy for $7a_1$, $8a_1$ and $1a_2$, respectively) contain unpaired electrons, all with parallel spin.

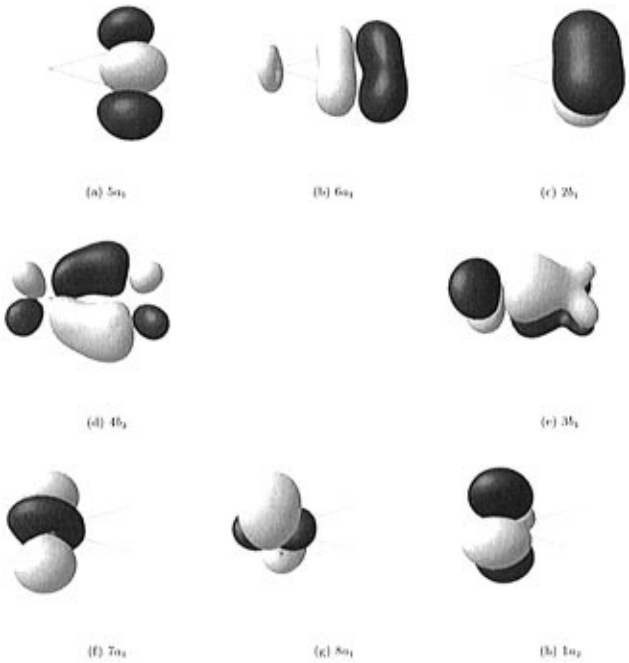

Figure 6. Chemically important CASPT2 canonical orbitals of quintet MoN_2. The $3b_1$, $7a_1$, $8a_1$, and $1a_2$ are singly occupied; the rest are doubly occupied.

TABLE 7: Classification of the Chemically Important MOs of Quintet MoN_2

orbital	electron count	N−N bonding	N_2−Mo bonding
$5a_1$	2	+1 (σ)	none
$6a_1$	2	+1 (π_z)	none
$2b_1$	2	+1 (π_x)	none
$4b_2$	2	−1 (π_z*)	+1
$7a_1$	1	none	lone electron
$8a_1$	1	none	lone electron
$1a_2$	1	none	lone electron
$3b_1$	1	>0 (π_x)	>0
total	12	>2	>1

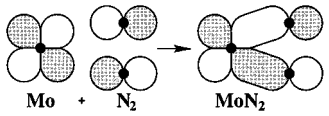

Figure 7. Combination of the Mo $4d_{yz}$ and N_2 in-plane $2p\pi$* orbitals into the $^5B_2$ MoN_2 $4b_2$ orbital.

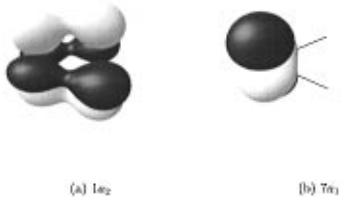

Figure 8. Doubly occupied CASPT2 canonical orbitals of $^1A_1$ MoN_2 that are discussed in the text.

In the narrow-angle $^1A_1$ singlet state of MoN_2 the $(5a_1)^2(6a_1)^2(2b_1)^2(4b_2)^2$ part remains occupied with little change in shape and occupation. The remaining four electrons from a $(1a_2)^2(7a_1)^2$ configuration (Figure 8). The former is a Mo−(N_2) δ bond with respect to the z axis. It makes Mo−N bonds and partially breaks the N−N off-plane $2p\pi$ bond. The $7a_1$ is a $4d_{x^2}$ lone-pair orbital. (Since we have no orbital energies available from the CASPT2 calculation, we have numbered the orbitals in decreasing order of occupation. The lone pair should, by its occupation, be called $5a_1$ in this species, but we retain the earlier nomenclature for easier discussion.)

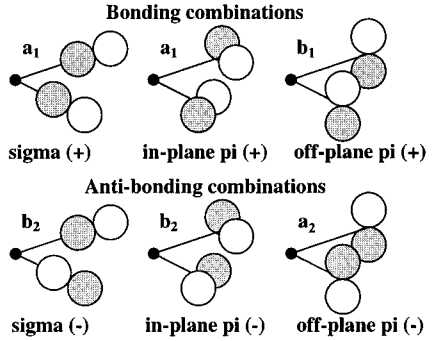

Figure 9. Possible combinations of the valence p orbitals of the nonmetal atoms.

TABLE 8: Classification of the Chemically Important MO's of Triplet MoN_2

orbital	electron	N (2p)	Mo (4d)	comments
$5a_1$	2	in-plane π +	x^2	Mo−N bonding
$6a_1$	2	σ +	$y^2 - z^2$	Mo−N bonding
$1a_2$	2	off-plane π −	xy	Mo−N bonding
$2b_1$	2	off-plane π +	xz	Mo−N antibonding
$4b_2$	2	in-plane π −	yz	Mo−N bonding
$7a_1$	1	none	x^2	"antibonding $5a_1$"
$5b_2$	1	σ −	none	lone electron
total	12			

Compared with the $^5B_2$ state, in the $^1A_1$ the N−N distance is lengthened (from 122 pm in $^5B_2$ to 148 pm in $^1A_1$), and the Mo−N distances are shortened (from 208 pm in $^5B_2$ to 176 pm in $^1A_1$, see also Table 3). Comparisons of these N−N distances with the experimental ones in hydrazine (single N−N bond, 145 pm[38]), diimide (double N=N bond, 123 pm[38]), and N_2 (triple bond, 110 pm[39]) appear to support the conclusion that we have approximately a double bond in the quintet and a single bond in the singlet.

Our analysis qualitatively agrees with the DFT one of Martínez et al.[13] One should bear in mind that b_1 and b_2 are interchanged and that our lowest a_1 orbital is not included in their analysis. As a difference, we would emphasize the N−N antibonding contribution of the doubly occupied $4b_2$ orbital (Figure 7) in the initial quintet minimum of MoN_2, while their work mentions the transfer of a single α electron to an unspecified antibonding orbital of N_2 as the initial step of the reaction.

The Open-Angle Case. This case can be best understood by considering the X np AOs in a local coordinate system (n = 2 for X = N and O, n = 3 for X = P). There is an in-plane np-π, off-plane np-π, and a np-σ along the X−M bond. All three can be coupled to even or odd combinations (denoted + and −, respectively) with respect to the xz plane. These six combinations are shown in Figure 9.

Taking the MoN_2 triplet ($2S + 1 = 3$) as an example, the approximate CASPT2 electron configuration becomes $(5a_1)^2(6a_1)^2(1a_2)^2(4b_2)^2(7a_1)^1(5b_2)^1$. These orbitals are also shown in Figure 10 and are characterized in Table 8. The approximate Mo−N bond order would lie between 1.5 and 2. In the singlet state, the same natural orbitals remain occupied, but the spins in the $(7a_1)^1(5b_2)^1$ are antiparallel, yielding a $^1B_2$ state instead of $^3B_2$.

In the MoO_2^{2+} and WO_2^{2+}, the larger electronegativity of oxygen (relative to N or P) causes the electrons to shift more away from the metal atom, populating the $5b_2$ MO instead of the $7a_1$ with two electrons. In this case, we can count six bonding MOs between the three atoms, resulting in two triple bonds between the metal and oxygen. Since the electron density is now shifted more toward oxygen, placing an unpaired electron

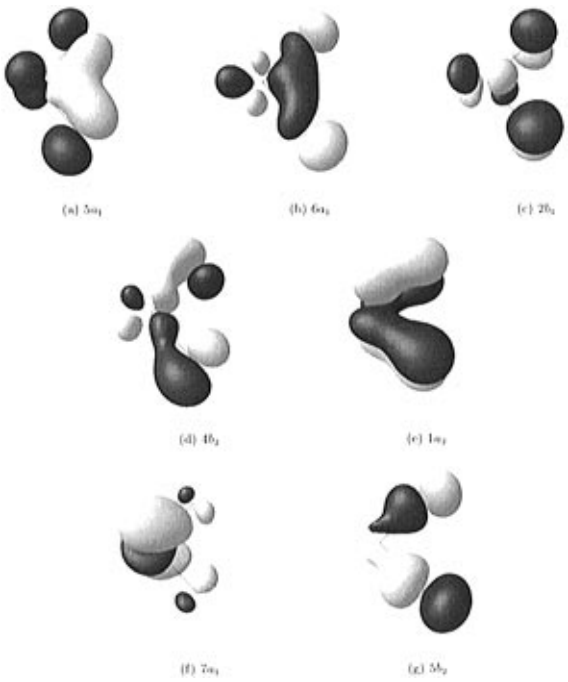

Figure 10. Chemically important CASPT2 canonical orbitals of triplet MoN_2. The $7a_1$ and $5b_2$ are singly occupied; the rest are doubly occupied.

on a d orbital of the metal would now be energetically unfavorable, which explains the absence of other states besides the $^1A_1$ on the studied potential energy surfaces of these species. Nominally MoO_2^{2+} is a d^0 species. In actual fact its MOs have substantial 4d character. A Mulliken analysis of the CASSCF orbitals gives a total 4d population of as much as $4d^{3.8}$. In the terminology of classical chemistry, of all the species studied, only the oxoions can be described with a single simple structure:

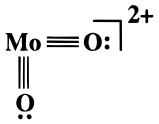

Thus the bonding of both the narrow-angle and wide-angle species can be understood in simple terms.

5. Conclusions

The free molybdenyl and tungstenyl groups, MoO_2^{2+} and WO_2^{2+}, have an autonomous existence. Their ground state is a singlet, and their geometries are close to those in the neutral MO_2X_2 oxyhalides.

The isoelectronic MN_2 dinitrides, and WP_2 diphosphides, exhibit multiple minima in their potential energy surfaces of different spin states. Both narrow (30−60°) and wide (90−110°) N−M−N or P−W−P bond angles can be found. In the narrow-angled geometries, some bonding remains between the N or P atoms, while in the wide-angled systems, the only bonding is between the metal and nonmetal.

Furthermore, it has not escaped our attention that the nitrogenase enzyme contains Mo and that the present structures of MoN_2, with the orbital structures described here, could possibly be seen as an important fragment in the transition state during the activation of N_2. The bonding analysis outlined above shows how the chemical bond in N_2 is weakened by occupation of the antibonding orbitals. In the complex surroundings of the enzyme, the relative location of the potential energy surfaces at various total spins could be very different from the one obtained in this grossly oversimplified model. The enzyme molybdenum atom is also not free, but bound to the reaction center by several chemical bonds. Nevertheless, it is not entirely excluded that the present singlet and triplet MoN_2 fragments might provide some insight into a potential working mechanism of nitrogenase.

Acknowledgment. This work was supported by The Academy of Finland. The calculations were performed on DEC AlphaStation 500/500 workstations of this laboratory, as well as on the SGI and DEC computers of the Center for Scientific Computing, Espoo, Finland. We are also grateful to Nino Runeberg, Dage Sundholm, and the entire group of Markku Räsänen for valuable discussions.

References and Notes

(1) Cotton, F. A.; Wilkinson, G. *Advanced Inorganic Chemistry*, 5th ed.; John Wiley & Sons: New York, 1988.
(2) Abel, E. W., Stone, F. G. A., Wilkinson, G., Eds. *Comprehensive Organometallic Chemistry II*; Elsevier: Amsterdam, 1995; Vol. 5.
(3) Wilkinson, G. F., Ed. *Comprehensive Coordination Chemistry*; Pergamon Press: Oxford, 1987; Vol. 3.
(4) Tatsumi, K.; Hoffmann, R. *Inorg. Chem.* **1980**, *19*, 2656−2658.
(5) Deeth, R. J. *J. Phys. Chem.* **1994**, *97*, 11625−11627.
(6) Fiedler, A.; Kretzschmar, I.; Schröder, D.; Schwarz, H. *J. Am. Chem. Soc.* **1996**, *118*, 9941−9952.
(7) Borrmann, H. Private communication.
(8) Laplaza, C. E.; Davis, W. M.; Cummins, C. C. *Angew. Chem., Int. Ed. Engl.* **1995**, *34*, 2042−2044.
(9) Zanetti, N. C.; Schrock, R. R.; Davis, W. M. *Angew. Chem., Int. Ed. Engl.* **1995**, *34*, 2044−2046.
(10) Wheeler, R. A.; Hoffmann, R.; Strähle, J. *J. Am. Chem. Soc.* **1986**, *108*, 5381−5387.
(11) Neuhaus, A.; Veldkamp, A.; Frenking, G. *Inorg. Chem.* **1994**, *33*, 5278−5286.
(12) Cui, Q.; Musaev, D. G.; Svensson, M.; Sieber, S.; Morokuma, K. *J. Am. Chem. Soc.* **1995**, *117*, 12366−12367.
(13) Martínez, A.; Köster, A. M.; Salahub, D. R. *J. Phys. Chem. A* **1997**, *101*, 1532−1542.
(14) Lide, D. R., Ed. *CRC Handbook of Chemistry and Physics*, 74th ed.; CRC Press: Boca Raton, FL, 1993−1994.
(15) Foosnaes, T.; Pellin, M. J.; Gruen, D. M. *J. Chem. Phys.* **1983**, *76*, 2889−2898.
(16) Lian, L.; Mitchell, S. A.; Rayner, D. M. *J. Phys. Chem.* **1994**, *98*, 11637−11647.
(17) Goldberg, K. I.; Hoffman, D. M.; Hoffmann, R. *Inorg. Chem.* **1982**, *21*, 3863−3868.
(18) Chertihin, G. V.; Andrews, L.; Neurock, M. *J. Phys. Chem.* **1996**, *100*, 14609−14617.
(19) Zacarías, A.; Torrens, H.; Castro, M. *Int. J. Quantum Chem.* **1997**, *61*, 467−473.
(20) Dasent, W. E. *Nonexistent Compounds: Compounds of Low Stability;* Marcel Dekker, Inc.: New York, 1965.
(21) Andrews, L. Private communication.
(22) Andersson, K.; Blomberg, M. R. A.; Fülscher, M. P.; Kellö, V.; Lindh, R.; Malmqvist, P.; Noga, J.; Olsen, J.; Roos, B. O.; Sadley, A. J.; Siegbahn, P. E. M.; Urban, M.; Widmark, P.-O. *MOLCAS*, version 3; University of Lund: Sweden 1994.
(23) Frisch, M. J.; Trucks, G. W.; Schlegel, H. B.; Gill, P. M.; Johnson, B. G.; Robb, M. A.; Cheeseman, J. R.; Keith, T. A.; Peterson, G. A.; Montgomery, J. A.; Raghavachari, K.; Al-Laham, M. A.; Zakrzewski, V. G.; Ortiz, J. V.; Foresman, J. B.; Cioslowski, J.; Stefanov, B. B.; Nanayakkara, A.; Challacombe, M.; Peng, C. Y.; Ayala, P. Y.; Chen, W.; Wong, M. W.; Andres, J. L.; Reploge, E. S.; Gomperts, R.; Martin, R. L.; Fox, D. J.; Binkley, J. S.; Detrees, D. J.; Baker, J.; Stewart, J. P.; Head-Gordon, M.; Gonzalez, C.; Pople, J. *Gaussian 94*; Gaussian, Inc. Pittsburgh, PA, 1994.
(24) Andrae, D.; Häussermann, U.; Dolg, M.; Stoll, H.; Preuss, H. *Theor. Chim. Acta (Berlin)* **1990**, *77*, 123−141.
(25) Dunning, T. H., Jr.; Hay, P. J. In *Modern Theoretical Chemistry*; Schaefer, H. F., III, Ed.; Plenum: New York, 1977; Vol. 3, Chapter 1, pp 1−28.
(26) Hay, P. J.; Wadt, W. R. *J. Chem. Phys.* **1985**, *82*, 299−310.
(27) Ehlers, A. W.; Böhme, M.; Dapprich, S.; Gobbi, A.; Höllwarth, A.; Jonas, V.; Köhler, K. F.; Stegmann, R.; Veldkamp, A.; Frenking, G. *Chem. Phys. Lett.* **1993**, *208*, 111−114.
(28) Huzinaga, S., Ed. *Gaussian Basis Sets for Molecular Calculations*; In Physical Sciences Data 16; Elsevier: Amsterdam, 1984.
(29) Andersson, K.; Malmqvist, P.-Å.; Roos, B. O.; Sadlej, A. A.; Wolinski, K. *J. Phys. Chem.* **1990**, *94*, 5483−5488.

(30) Andersson, K.; Malmqvist, P.-Å.; Roos, B. O. *J. Chem. Phys.* **1992**, *96*, 1211−1226.

(31) Andersson, K.; Malmqvist, P.-Å.; Roos, B. O.; Widmark, P.-O. *Chem. Phys. Lett.* **1994**, *230*, 391−397.

(32) AVS. 1989−1994, Advanced Visual Systems Inc.

(33) Lee, T. J.; Taylor, P. R. *Int. J. Quantum Chem., Quantum Chem. Symp.* **1989**, *23*, 199−207.

(34) Schrock, R. R. *Acc. Chem. Res.* **1997**, *30*, 9−16.

(35) Thomassen, H.; Hedberg, K. *J. Mol. Struct.* **1992**, *273*, 197−206.

(36) Jarchow, O.; Schröder, F.; Schultz, H. *Z. Anorg. Allg. Chem.* **1968**, *363*, 58−72.

(37) Moore, C. E. *Atomic Energy Levels*; National Bureau of Standards: Washington, DC, 1958; Vol. III.

(38) Wells, A. F. *Structural Inorganic Chemistry*, 5th ed.; Clarendon Press: Oxford, 1984.

(39) Huber, K. P.; Herzberg, G. *Molecular Spectra and Molecular Structure*; Van Nostrand Reinhold Company: New York, 1979; Vol. 4.